The impact of Mg^{2+} ions on equilibration of Mg−Ca carbonates in groundwater and brines

Preprint version of the article published in Geochemistry - Chemie der Erde,

https://doi.org/10.1016/j.chemer.2020.125611

Peter Möller[a], Marco De Lucia[a]

[a]*Helmholtz Centre Potsdam, GFZ German Research for Geosciences, Section 3.4 Fluid Systems Modelling, Telegrafenberg, 14473 Potsdam, Germany*

Abstract

At temperatures below 50 °C, the $\log_{10}({}^{a}Mg^{2+}/{}^{a}Ca^{2+})$ values in groundwater and brines, irrespective of their origin - either carbonaceous or siliceous rocks/sediments - cover the range between -1.5 and +1.0. Calculations of thermodynamic equilibria between the minerals calcite, aragonite, dolomite and huntite suggest a spread of $\log_{10}({}^{a}Mg^{2+}/{}^{a}Ca^{2+})$ between minus infinity and +2.3. $\text{Log}_{10}({}^{a}Mg^{2+}/{}^{a}Ca^{2+})$ in solution of dissolving ordered dolomite at 25 °C fits the thermodynamical equilibrium between disordered dolomite and calcite and nearly corresponds to that of pure calcite with a dolomitic surface layer due to exchange of Ca^{2+} against Mg^{2+} in Mg^{2+}-containing solutions. This observation suggests that the solubility of Mg-Ca carbonates is controlled by the composition of their monomolecular surface layers in equilibrium with the ambient aqueous phase. Incongruently dissolving minerals such as dolomite attain equilibrium between individual surface compositions of different carbonates. The bulk composition of these carbonates hardly if ever equilibrates with the ambient solution due to extremely low ion mobility in the lattice. Because the thermodynamical equilibria are based on the composition of bulk minerals, their estimates of equilibria between carbonates, i.e., $\log_{10}({}^{a}Mg^{2+}/{}^{a}Ca^{2+})$ in solution, differ significantly from values established by the chemical composition and structure of the surface layer of carbonates.

Keywords: Magnesian calcite, Dolomite, Dissolution of carbonates, Thermodynamics of carbonates, Surface composition of carbonates

1. Introduction

Ca^{2+} and Mg^{2+} are very important in carbonate geochemistry with several yet unexplainable features. Ca-Mg minerals with Mg^{2+}/Ca^{2+}=1 and 3, i.e., dolomite and huntite, are formed in nature but the absence of a mineral with Mg^{2+}/Ca^{2+}=2 is striking. Surface complexes such as aquacomplexes, $>Mg^{2+}-H_2O$, may play a role but cannot explain the absence of a carbonate with the Mg^{2+}/Ca^{2+} surface ratio of 2. Why is the formation of dolomite at ambient temperatures difficult or even impossible, well-known as the dolomite problem (Gregg et al., 2015)? The dolomite problem has been controversially debated over the last 100 years. Although our knowledge about physico-chemical processes in carbonate geochemistry has improved with time we still lack final answers (refer to Gregg et al., 2015; Raiteri et al., 2015). Besides the high abundance of carbonate rocks in nature calcite also forms along with weathering of all kind of Ca^{2+}-bearing rocks. Studying the Mg^{2+} exchange against Ca^{2+} at surfaces of calcite powders and single crystals reveals that the Mg^{2+} exchange had some impact on calcite solubility but is insignificant with respect to changes in Mg^{2+} activity in solution (Möller, 1973; Koss and Möller, 1974; Pokrovsky et al., 2009a).

Besides hydrated metastable phases, a wide variation in composition of Mg-Ca carbonates occurs in nature between the possible endmembers calcite and magnesite (Table 1). Low magnesian calcite (LMC) precipitates inorganically, whereas high magnesian calcite (HMC) is either of biogenic or diagenetic origin. Nesquehonite but not magnesite forms at ambient temperatures (Davies and Bubela, 1973; Zachmann, 1989) (Table 1). The experimental formation of dolomite below temperatures of about 50 °C is impeded by kinetics because of lacking the necessary activation energy needed for fully dehydration of Mg^{2+} in dolomite nuclei (Gregg and Sibley, 1984; Land, 1998; Arvidson and Mackenzie, 1999; Mavromatis et al., 2013; Baldermann et al., 2015; Wang et al., 2016; Perez-Fernandez et al., 2017). Alternatively, the inhibited growth of dolomite is explained by deposition of a "poorly ordered dolomite-like phase

that poisons the surface" (Berninger et al., 2017). In nature, however, dolomite seemingly forms below 50 °C but its formation is not fully understood yet (Gregg et al., 2015). Although HMC and VHMC/proto-dolomite (Table 1) are metastable, they are known to survive geological times (Land, 1985). These metastable products occur side by side together with ordered dolomite without establishing bulk equilibria (Brätter et al., 1972; Warren, 2000).

Mineral	**Abbr.**	**Composition**	**mol-%** $MgCO_3$
Calcite		$CaCO_3$	0
Aragonite		$CaCO_3$	0
Low Mg calcite	LMC	$Ca_yMg_{(1-y)}CO_3$	<4
High Mg calcite	HMC	$Ca_yMg_{(1-y)}CO_3$	4-30
Very high Mg calcite	VHMC	$Ca_yMg_{(1-y)}CO_3$	30-45
Disordered dolomite = proto dolomite		$Ca_xMg_{(2-x)}(CO_3)_2$	46-50
Ordered dolomite		$Ca_xMg_{(2-x)}(CO_3)_2$	46-50
Huntite		$CaMg_3(CO_3)_4$	75
Nesquehonite		$MgCO_3 * 3H_2O$	100
Hydromagnesite		$Mg_5[OH/(CO_3)_2]_2$	100
Magnesite		$MgCO_3$	100

Table 1: *Ca-Mg carbonates, their chemical formula and the mol-%* $MgCO_3$*. The subscripts* x *and* y *express the deviation from the stoichiometric coefficients of endmembers calcite and dolomite, respectively; both are one for the perfectly stoichiometric phases.*

The Mg^{2+} ions inhibit growth of calcite by increasing its solubility due to incorporation of Mg^{2+} into the calcite lattice (Plummer and Mackenzie, 1974; Thorstenson and Plummer, 1977; Mucci and Morse, 1983; Davis, 2000) and exchange of Mg^{2+} against Ca^{2+} in calcite surface layers (Koss and Möller, 1974). Under increased activities of Mg^{2+} in Ca^{2+}-bearing solutions, also aragonite precipitates (Kitano et al., 1962). The calcite growth rate decreases in presence of Mg^{2+} and SO_4^{2-} (Pokrovsky, 2001; Pokrovsky et al., 2005, 2009a,b; Gledhill and Morse, 2006; Nielsen et al., 2016), which both enhances the hydrophilic character of the calcite surface and weakens the adsorption of organic compounds (Generosi et al., 2016; Andersson et al., 2016). Besides inorganic components, also organic components inhibit growth of calcite such as citrate (Montanari et al., 2017), alginate (Lakshtanov et al., 2014) and acetate (Dobberschütz et al., 2018).

The aim of this contribution is to decipher the conditions under which differently composed Mg-Ca carbonates equilibrate in aqueous solutions. An answer is approached by comparing thermodynamically and analytically derived ratios of Mg^{2+} and Ca^{2+} in ambient solutions in contact with both calcite and dolomite.

2. Thermodynamic approaches to Mg^{2+}/Ca^{2+} at equilibria of carbonates

Thermodynamics suggest that the carbonate equilibria compiled in Table 2 are given by the activity ratio of Mg^{2+} and Ca^{2+} (Eq. 1). The activities of the solids are taken as unity. Depending on the thermodynamic data sets different temperature-dependent trends for ordered dolomite-calcite and disordered dolomite-calcite are derived (Fig. 1). These equilibria are calculated using the freely available CHNOSZ package (Dick, 2019) which implements both the Berman and Brown (1985) model for aqueous species and minerals and the revised Helgeson-Kirkham-Flowers's (Helgeson et al., 1981) equations for aqueous species. The equilibrium of various carbonates expressed as $\log_{10}({}^{a}Mg^{2+}/{}^{a}Ca^{2+})$ are therefore based on 3 different thermodynamic databases and their underlying formalisms,

1. the compilations of Berman (1988),
2. the compilation of Helgeson et al. (1978), of Plummer and Busenberg (1982) and of Berman (1988) with many successive integrations, and
3. where the necessary data are not available in the above compilations, such as disordered dolomite, data on dissolution of minerals are extracted from the "llnl.dat" database distributed with PHREEQC 3.4.0 (Appelo et al., 2014).

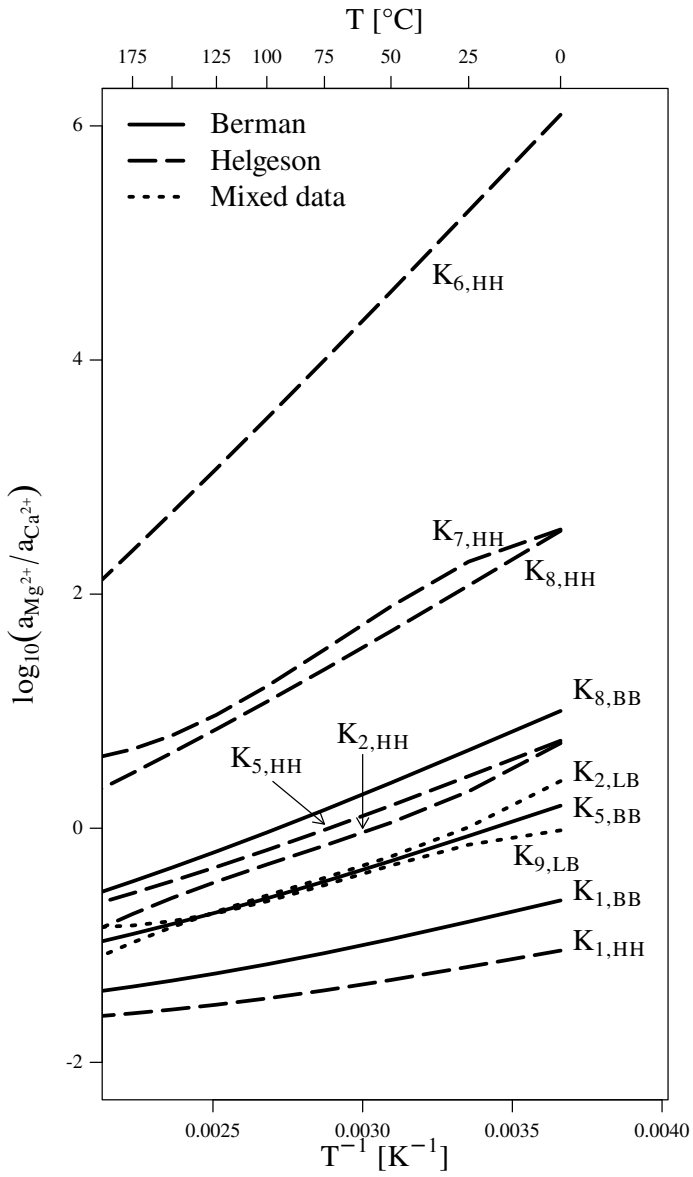

Fig. 1: *Thermodynamic estimates of mineral equilibria in the temperature range of 0–175 °C. In the indices of K, the figures refer to the reaction in Table 2; capital letters indicate the sources of thermodynamic data of the educt and product in the corresponding reaction:* BB, *both are from Berman (1988);* HH, *both are from Helgeson et al. (1978);* LB, *data for the educt data are taken from "llnl.dat" data base (Appelo et al., 2014) and the product data from Berman (1988). These line types are used in the following plots.*

Id	Reaction	Data source	
		educt	product
K_1	Calcite to dolomite	$2CaCO_3 + Mg^{2+} = CaMg(CO_3)_2 + Ca^{2+}$	B,H,L	B,H,L
K_2	Calcite to disordered dolomite	$2CaCO_3 + Mg^{2+} = CaMg(CO_3)_2 + Ca^{2+}$	B,H,L	L
K_3	Aragonite to dolomite	$2CaCO_3 + Mg^{2+} = CaMg(CO_3)_2 + Ca^{2+}$	B,H,L	B,H,L
K_4	Aragonite to disordered dolomite	$2CaCO_3 + Mg^{2+} = CaMg(CO_3)_2 + Ca^{2+}$	B,H,L	L
K_5	Calcite to magnesite	$CaCO_3 + Mg^{2+} = MgCO_3 + Ca^{2+}$	B,H,L	B,H,L
K_6	Dolomite to huntite	$2CaMg(CO_3)_2 + Mg^{2+} = CaMg_3(CO_3)_4 + Ca^{2+}$	H,L	H,L
K_7	Disordered dolomite to huntite	$2CaMg(CO_3)_2 + Mg^{2+} = CaMg_3(CO_3)_4 + Ca^{2+}$	L	H,L
K_8	Dolomite to magnesite	$CaMg(CO_3)_2 + Mg^{2+} = 2MgCO_3 + Ca^{2+}$	B,H,L	B,H,L
K_9	Disordered dolomite to magnesite	$CaMg(CO_3)_2 + Mg^{2+} = 2MgCO_3 + Ca^{2+}$	L	B,H,L
K_{10}	Dolomite to nesquehonite	$CaMg(CO_3)_2 + Mg^{2+} + 3H_2O = 2MgCO_3 : 3H_2O + Ca^{2+}$	B,H,L	B,H,L
K_{11}	Disordered dolomite to nesquehonite	$CaMg(CO_3)_2 + Mg^{2+} + 3H_2O = 2MgCO_3 : 3H_2O + Ca^{2+}$	L	B,H,L

Table 2: *Compilation of considered reactions, their Gibbs free energies and the* $\log_{10}({}^{a}Mg^{2+}/{}^{a}Ca^{2+})$ *at equilibrium at 25°C assuming that the activities of the solids approach unity.*

Id		Reaction
K_{12}	Magnesite dissolution	$MgCO_3 + H^+ = Mg^{2+} + HCO_3^-$
K_{13}	Huntite dissolution	$CaMg_3(CO_3)_4 + 4H^+ = Ca^{2+} + 3Mg^{2+} + 4HCO_3^-$
K_{14}	Aragonite dissolution	$CaCO_3 + H^+ = Ca^{2+} + HCO_3^-$
K_{15}	Calcite dissolution	$CaCO_3 + H^+ = Ca^{2+} + HCO_3^-$
K_{16}	Disordered dolomite dissolution	$CaMg(CO_3)_2 + 2H^+ = Ca^{2+} + Mg^{2+} + 2HCO_3^-$

Table 3: *Compilation of mineral dissolution reactions needed to estimate K_i in Table 2 with $i = 2, 4, 7, 9$ and 11.*

Note that the dissolution reactions $i = 12 - 16$ in Table 3 are needed to evaluate the reaction constant $\log_{10} K_i$ with $i = 2, 4, 7, 9$ and 11 the reactions in which disordered dolomite is involved.

Fig. 1 displays the temperature-dependent equilibria of all considered mineral equilibria in Table 2. Note the discrepancies between equilibria based on thermodynamical data of Berman (1988) and those of Helgeson et al. (1978). Since Berman followed chronologically Helgeson et al. (1981) and partially revised their approach, we consider his data most reliable. It has to be noted that mixing data may introduce additional inconsistencies in the calculations.

The equilibrium of the substoichiometrically composed magnesian calcite and dolomite, with the same subscript convention adopted in Table 1, is expressed in Eq. (1). $Log_{10}K_{x/y}$ (Eq. 2) is derived from Eq. (1). Eq. (2) can be developed into Eq. (3) in terms of free energy of reaction. The indices x and y indicate the surface composition of dolomite and calcite, respectively.

$$2Ca_yMg_{(1-y)}CO_3 + (2y-x) \cdot Mg^{2+} = Ca_xMg_{(2-x)}(CO_3)_2 + (2y-x) \cdot Ca^{2+} \quad (1)$$

$$\log_{10} K_{x/y} = -(2y-x) \log_{10} \frac{{}^aMg^{2+}}{{}^aCa^{2+}} + \log_{10} \frac{\{{}^adol_x\}}{\{{}^aCc_y\}^2} \quad (2)$$

$$\frac{\Delta_r G}{\ln(10)RT} = (2y-x) \log_{10} \frac{{}^aMg^{2+}}{{}^aCa^{2+}} + \log_{10} \frac{\{{}^aCc_y\}^2}{\{{}^adol_x\}} \quad (3)$$

The assumption of equilibrium for the reaction of Eq. (1) results in Eq. (4):

$$\log_{10} \frac{{}^aMg^{2+}}{{}^aCa^{2+}} = \frac{1}{2y-x} \log_{10} \frac{\{{}^adol_x\}}{\{{}^aCc_y\}^2} \quad (4)$$

Thus, the activity ratio of Mg^{2+} and Ca^{2+} in solution depends on the stoichiometric factors of magnesian calcite and disordered dolomite and on the activity ratio of the surface phases ${}^adol_x$ and the square of $\{{}^aCc_y\}^2$. If ${}^aMg^{2+}/{}^aCa^{2+}=1$, it follows from Eq. (4):

$$\{{}^adol_x\}=\{{}^aCc_y\}^2 \quad (5)$$

3. The impact of Mg^{2+} on calcite solubility

3.1. Results on Ca^{2+}-Mg^{2+} exchange at calcite surfaces

The here summarized analytical method is much more precise than any X-ray photoelectron spectrometric one because the former gives direct insight into a single molecular surface layer, whereas the latter only allows the determination of the average composition of surface layers of 80 to 100 Å thickness, which amounts to about 20 to 25 layers of carbonates. Spectrometric data thus represent the composition of the underlying carbonate layers and do not justify the conclusion of Pokrovsky (2001) that the surface composition of dolomite stays constant in experiments with varying Ca^{2+} and Mg^{2+} concentrations. The ion exchange, however, is restricted to about one molecular layer as proved by experiments on single crystals (Möller and Sastri, 1974).

Distilled water was saturated with respect to reagent grade $CaCO_3$ p.a. (Merck®) or single crystals of calcite for periods of 10 days at temperatures between 20-25 °C and atmospheric pCO_2. The 4

µm filtered calcite-saturated solution was spiked with ^{45}Ca (β-decay with half-life of 163.8 days). The equilibrated calcite was placed in the spiked solution for at least 15 hours, where it underwent ion exchange of $^{45}Ca^{2+}$ against Ca^{2+} in the calcite surface. Thereafter the calcite was separated from its solution, cleaned with distilled water, dried, and the β-activity was determined by low β-proportional counting assembly (Möller and Sastri, 1974; Sastri and Möller, 1974). Thereafter the ^{45}Ca spiked solids were placed into a calcite-saturated solution to which a small amount of $MgCl_2$ was added. After 15 hours the calcite was washed and dried for β counting. This procedure is repeated with increasing amounts of $MgCl_2$ in calcite saturated solutions (Möller and Rajagopalan, 1972; Möller, 1973). In these Mg^{2+} containing solutions calcite underwent exchange of surface Ca^{2+} ions against Mg^{2+} and $^{45}Ca^{2+}$ decreased in the calcite surface. With increasing Mg^{2+}concentrations in solution the Mg^{2+}/Ca^{2+} in the surface layer of stoichiometric calcite increased systematically to of 1:1 and with further increasing $(Mg^{2+}/Ca^{2+})_{soln}$ to 3:1. The ratio of 2:1 is not indicated by a change of slope (Fig. 2a, b). The ion exchange at surfaces of single crystals of calcite revealed that only one surface layer was involved in this exchange reaction (Möller and Sastri, 1974).

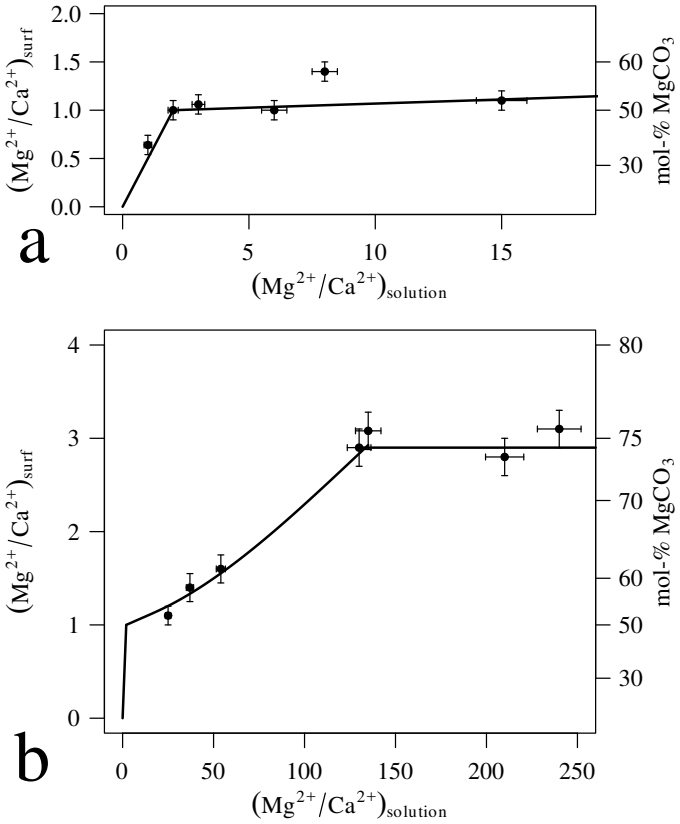

Fig. 2: *Surface exchange of* Ca^{2+} *against* Mg^{2+} *in the monomolecular surface layer calcite (a; b). Data are taken from Möller (1973) and Möller and Sastri (1974).*

Mg^{2+} has a strong tendency to replace Ca^{2+} because the former is more strongly bound in the calcite surface than the latter (Möller, 1973). In presence of Mg^{2+}, the Ca^{2+} concentration increases in solution. The negative logarithm of the ion activity product, $p(IAP)_{Cc_y}$, decreases with increasing Mg^{2+}/Ca^{2+} in calcite surface (Fig. 3). For calcite with surface composition between 0 and 50 mol-% $MgCO_3$ $p(IAP)_{Cc_y}$ at 25 °C and atmospheric CO_2 decreases from 8.4 (Plummer and Mackenzie, 1974) to 8.2. For comparison, ordered dolomite ($Ca_{0.5}Mg_{0.5}CO_3$) in 0.1 M NaCl solution, atmospheric CO_2 at 25 °C shows $0.5p(IAP)_{dol}$ of 8.6 (Bénézeth et al., 2018) which is more than that of the dolomitic-composed calcite surface of 8.2.

After reaching the surface composition of 50 mol-% $MgCO_3$, $p(IAP)_{Cc_y}$ increases toward the huntitic surface composition of calcite ($Mg_{0.75}Ca_{0.25}CO_3$) at Mg^{2+}/Ca^{2+} at about 250 (Fig. 2) the estimated ion activity product $p(IAP)_{Cc_y}$ decrease to about 7.0. This decrease in $p(IAP)_{Cc_y}$ is only observed for ion

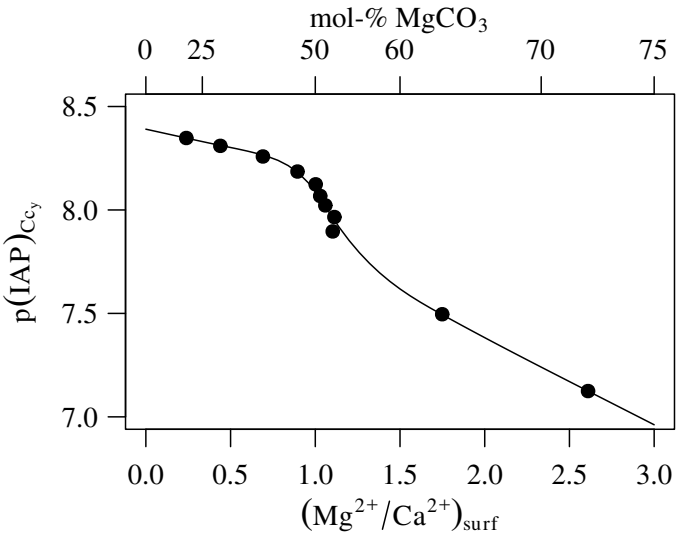

Fig. 3: *Estimated ion activity product,* $p(IAP)_{Cc_y}$*, of pure calcite as a function of* Mg^{2+}/Ca^{2+} *surface composition after Koss and Möller (1974).*

exchange of Mg^{2+} against Ca^{2+} in calcite surfaces. In the exchange Fe^{2+}, Co^{2+} and Ni^{2+} against Ca^{2+} the corresponding $p(IAP)_{Cc_y}$ values increase (Koss and Möller, 1974).

As a consequence of the ion exchange of Mg^{2+} against Ca^{2+} the adjacent planar CO_3^{2-} ions rotate accommodating the smaller Mg^{2+} ion (Fig. 4). The surface-bound Mg^{2+} shows a lower enthalpy than its Ca^{2+} counterpart (Möller and Rajagopalan, 1976) and the surface exchange of Mg^{2+} against Ca^{2+} spontaneously occurs with loss of free energy. The initial, probably statistical distribution of Mg^{2+} in the surface rearrange into a systematic one, in which the separate alignment of Mg^{2+} and Ca^{2+} ion is energetically favoured. The surface probably displays a mosaic structure of a 2-dimensional dolomitic layer.

3.2. Low-temperature dependence of carbonate equilibria

In the following, different groundwaters and brines from study areas in Israel, Jordan and the North German Basin are summarized in Fig. 5. In spite of the varying mineralogical composition of rocks acting as catchment and/or aquifer one would expect high variations in Mg^{2+}/Ca^{2+}; however, it is evident that Mg^{2+}/Ca^{2+} values in fluids do not scatter very much irrespective of the dominant lithologies (Table 4). The samples in Fig. 5d are from four totally different regions around the world and not from carbonate-dominated lithologies. Nevertheless these samples cover the same spread of ratios as the former ones. Groundwater and brines in Table 4 are grouped with respect to their lithological sources such as the Arabian platform carbonates (Fig. 5a,b), platform carbonates with local cover of alkali olivine basalts (Fig. 5c), and miscellaneous sources such as Pleistocene sediments in northern Germany, springs and wells in the Hauran Plateau/Syria (Cretaceous limestones covered by basalts) and springs discharging from the sediments of the Altiplano/Chile (Fig. 5d). The chemical analyses of groundwater and brines are shown in Appendix A together with the activities of Mg^{2+} and Ca^{2+}, estimated by PHREEQC applying the "llnl.dat" and "pitzer.dat" in PHREEQC (Appelo et al., 2014).

The change of $Mg^{2+}-Cl^-$ brine of the Ha'On well to $Ca^{2+}-Cl^-$ brine at Tiberias, both localities being separated by Lake Tiberias, Israel, is of particular interest (Fig. 5a). Their Na^+/Cl^- and Br^-/Cl^- are very similar in both types of brines and resemble evaporated seawater (Möller et al., 2011). The Ha'On water samples originate from Cretaceous limestone aquifers that were infiltrated by Late Tertiary evaporated seawater (Möller et al., 2018). Its $\log_{10}({}^{a}Mg^{2+}/{}^{a}Ca^{2+})_{soln}$ value plot near to the equilibrium of disordered dolomite and calcite (after Helgeson et al., 1981). With $(Mg^{2+}/Ca^{2+})_{soln}$ of 2.6, the calcite surface has a dolomitic composition (Fig. 2a) but the mineral dolomite has not to be present because of the low temperature of this brine. This dolomitic surface composition mimics the presence of disordered dolomite.

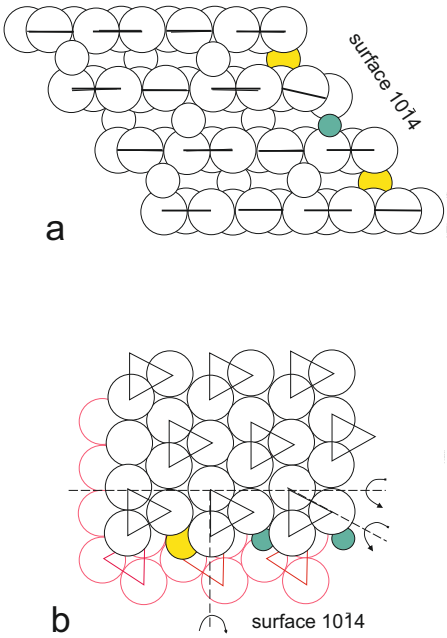

Fig. 4: *Schematic cross section (a) and view onto a carbonate plain of calcite (b) showing the structural changes following the exchange of* Ca^{2+} *against* Mg^{2+} *in calcite surface after Möller and Rajagopalan (1972).*

The Tiberias Hot Springs' (THS) brines originate from Jurassic/Cretaceous carbonate aquifers consisting of dolomite and limestone. The lower $\log_{10}({}^{a}Mg^{2+}/{}^{a}Ca^{2+})_{soln}$ than in Ha'On brine is the result of dolomitization of limestone by which Mg^{2+} is consumed and Ca^{2+} is released. The necessary, enhanced temperature to overcome the activation energy of dehydration of Mg^{2+} was supplied by abundant fissures and dykes of olivine basalts in these carbonate rocks. This interpretation is in agreement with PHREEQC inverse modelling (Möller et al., 2011). The final $(Mg^{2+}/Ca^{2+})_{soln}$ of 0.32 indicate similar surface activities of dolomite and calcite. Calcite shows $(Mg^{2+}/Ca^{2+})_{surf}$ of 0.16 (Fig. 2a). The dolomite surface is suspected to show $(Mg^{2+}/Ca^{2+})_{surf}$ >1. This example reveals that $(Mg^{2+}/Ca^{2+})_{soln}$ of carbonates solely depends on their surface composition and not on the bulk composition of minerals. The $\log_{10}({}^{a}Mg^{2+}/{}^{a}Ca^{2+})_{soln}$ do not allow identification of carbonate minerals involved by means of thermodynamic considerations. Although here only the influence of Mg^{2+} in solutions is discussed, it should be mentioned that also Fe^{2+} and many other inorganic and organic species vary the solubility of calcite under reducing conditions (Koss and Möller, 1974; Pokrovsky et al., 2009a).

The groundwater of the Hauran Plateau in Syria originate from springs discharging from the alkaline olivine basaltic cover or is exploited from the underlying Cretaceous limestones. The spring water shows lower $\log_{10}({}^{a}Mg^{2+}/{}^{a}Ca^{2+})_{soln}$ than the water from the limestone aquifer because the top basalts have lost its olivine already by weathering. This is different for the deep basalts, where weathering of olivine is still going on. These waters also infiltrate the underlying limestones, whereby high $\log_{10}({}^{a}Mg^{2+}/{}^{a}Ca^{2+})_{soln}$ values are established. The interaction of the Mg^{2+}-rich water from the top of limestones reduces the Mg^{2+} concentration due to surface exchange of Ca^{2+} against Mg^{2+}. Similar trend is to be seen in the low-temperature water from the Golan and Ajloun, where rain water infiltrates through basaltic rocks into underlying Cretaceous limestones. Weathering solution of siliceous rocks or sediments show a wide spread in $\log_{10}({}^{a}Mg^{2+}/{}^{a}Ca^{2+})_{soln}$ (Fig. 5d). Ca^{2+} is largely determined by calcite precipitation. Mg^{2+} in such solutions depends on reactions in which Mg^{2+} is involved such as the formation of clay minerals.

In general the spread of temperature-dependent $\log_{10}({}^{a}Mg^{2+}/{}^{a}Ca^{2+})_{soln}$ of these groundwaters and brines plots between -1.5 and +1.0, which corresponds up to about 50 mol-% $MgCO_3$ in calcite surfaces (Fig. 2). The majority of samples plot below $\log_{10}({}^{a}Mg^{2+}/{}^{a}Ca^{2+})$ of zero thereby indicating surface compositions of calcite up to 40 mol-% of $MgCO_3$. Although the behaviour of magnesian calcite with respect to surface ion exchange of Ca^{2+} against Mg^{2+} has not been studied, it may be suspected that

$\log_{10}({}^{a}Mg^{2+}/{}^{a}Ca^{2+})_{soln}$ of magnesian calcite resembles those determined for the $Mg^{2+}-Ca^{2+}$ surface compounds on pure calcite as it will be shown later for ordered dolomite and the dolomitic surface composition on a calcite matrix (subsection 3.3). Here it should be noted that there is not much difference between concentration and activity ratios (Appendix A, Fig. A.1). $\text{Log}_{10}({}^{a}Mg^{2+}/{}^{a}Ca^{2+})_{soln}>0$ typify either weathering solutions from Mg^{2+}-rich igneous rocks or Mg^{2+}-rich evaporation brines such as the brines of the Dead Sea, Rift and Ha'On well (Fig. 5a) or some of the well waters from the Hauran Plateau/Syria (Fig. 5c), and few samples in Fig. 5d. $\text{Log}_{10}({}^{a}Mg^{2+}/{}^{a}Ca^{2+})_{soln}$ below $K_{1,HH}$ characterise liquids interacting with Mg-poor rocks such as amphibolites (e.g., KTB-VB; Möller et al., 2005). With few exceptions waters and brines plot between $K_{1,HH}$ and $K_{2,HH}$, most of them between $K_{2,LB}$ and $K_{1,LB}$ mimicking the presence of either ordered or disordered dolomite and HMC. At low temperatures, these phases cannot form but are represented by corresponding surface compositions of calcite. Note that the $\log_{10}({}^{a}Mg^{2+}/{}^{a}Ca^{2+})_{soln}$ rarely plot along the thermodynamical estimated trends. The majority of samples plot along curves subparallel to the given ones indicating abundant Mg^{2+}/Ca^{2+} values.

Groundwater and brines from the same region show temperature-dependent trends of $\log_{10}({}^{a}Mg^{2+}/{}^{a}Ca^{2+})_{soln}$ similar to those suggested by thermodynamic estimates (Fig. 5a: Red Sea; Fig. 5b: Meizar wells; Fig. 5d: Mississippi Salt dome basin). Their $\log_{10}({}^{a}Mg^{2+}/{}^{a}Ca^{2+})_{soln}$ at a given temperature may be different due to environmental conditions and presence of siliceous rocks or sediments from which Mg^{2+} is either gained or consumed.

The Mg^{2+}/Ca^{2+} of calcite surfaces reflect the non-linearity of Mg^{2+}/Ca^{2+} in solution (refer to to the step-like function in Fig. 2). There are no simple correlations between Mg^{2+}/Ca^{2+} in solution and the Ca^{2+}-Mg^{2+} mineralogy of either catchment or aquifer rocks. The analyses prove that the temperature-dependent Mg^{2+}/Ca^{2+} values plot in the array defined by thermodynamics (using the corresponding input data). These thermodynamic equilibrium lines are of course based on stoichiometric compositions of the carbonate minerals, thus not considering deviating surface compositions.

3.3. Temperature-dependent dissolution of dolomite

Dolomite dissolution experiments reported by Bénézeth et al. (2018) refer to about 3 g of freshly broken dolomite crystals of the composition $Ca_{1.04}Mg_{0.96}(CO_3)_2$ in 100 ml of 0.1 M NaCl solution. The incongruent dissolution of dolomite leads to solutions saturated with respect to calcite and $\log_{10}({}^{a}Mg^{2+}/{}^{a}Ca^{2+})_{soln}$ in equilibrium with the surface composition of both mineral phases dolomite and calcite. Scanning electron micrographs revealed precipitation of calcite and probably dolomite (Bénézeth et al., 2018). The amount of dolomite dissolving depends on the amount of solution. The resulting Mg^{2+} concentration in solution is independent on the amount of solution. Ca^{2+} increases in solution until precipitation of calcite; thereafter its concentration is constant. The extrapolated $\log_{10}(IAP)_{dol}$ at 25 °C is given by -17.2±0.3. This value is slightly higher than those derived from either "llnl" or "pitzer" databases. Reevaluation of the reported logarithms of Mg^{2+} and Ca^{2+} concentrations in 0.1 M NaCl solutions of dolomite at various pCO_2 and temperatures between 50 and 250 °C using either "llnl.dat" or "pitzer.dat" yields $\log_{10}(IAP)_{dol}$ at 25 °C of -17.8 and -17.5, respectively (Fig. 6). For more information refer to Appendix B.

The incongruent dissolution of dolomite increasing with temperature suggests that Mg^{2+} relative to Ca^{2+} increases in the reactive surface layer of dolomite, whereas the bulk composition of dolomite with 49.8 mol-% $MgCO_3$ does not change during dissolution. Although these solids precipitated, $\log_{10}({}^{a}Mg^{2+}/{}^{a}Ca^{2+})_{soln}$ decreased from about 0.08 at 50 °C to -0.47 at 250 °C suggesting significant changes of Mg^{2+}/Ca^{2+} in the surfaces of dolomite and calcite. With $Mg^{2+}>Ca^{2+}$ in solution any precipitation of LMC and dolomite increases $(Mg^{2+}/Ca^{2+})_{soln}$. The incongruent dissolution of dolomite yielding $\log_{10}({}^{a}Mg^{2+}/{}^{a}Ca^{2+})_{soln}$ of 0.08 at 50 °C (Fig. 6) indicates that the surface composition of dolomite shows $Mg^{2+}/Ca^{2+}>1$. With increasing temperature the difference between the thermodynamic equilibrium of disordered dolomite and calcite and their Mg^{2+}/Ca^{2+} in solution increases which is due to increasing amounts of precipitated LMC. Above about 150 °C the solubility of calcite increases and thus $\log_{10}({}^{a}Mg^{2+}/{}^{a}Ca^{2+})_{soln}$ decreases.

In view of Fig. 6, the published pIAP values of dolomite refer to the equilibrium of disordered dolomite and calcite, in other words, there is neither congruent dissolution of ordered dolomite nor equilibrium between ordered dolomite and calcite. Although the surfaces of both mineral phases are differently composed, they are in equilibrium with the same Mg^{2+}/Ca^{2+} composition in solution. The $p(IAP)_{dol}$ =17.2±0.3 after Bénézeth et al. (2018) differs by about 0.8 log units (subsection 3.1) from $p(IAP)_{Cc_y}$

Fig	Sources of water/brines	Lithology	Reference
5a	Jordan-Dead Sea Rift/ Israel		
	Ha'On well	Cretaceous limestones	Möller et al. (2009), Bergelson et al. (1999)
	Tiberias Hot Springs	Cretaceous limestones/dolostones	"
	Dead Sea	"	Krumgalz (1997)
	Red Sea Graben Brines	Oceanic basalts; metalliferous sediments	Pierret et al. (2001)
5b	Yarmouk Gorge/Israel, Jordan		
	Springs at Hammat Gader, Israel	Limestones	Siebert et al. (2014)
	Mezar well field, Israel	Limestones	"
	Ain Himma, Jordan	Limestones	"
	Mukheibeh Well Field, Jordan	Limestones	"
5c	Yarmouk basin		
	Wells in the Ajloun, Jordan	Limestones and basalts	Siebert et al. (2014)
	Well in the Golan Heights	Limestones and basalts	"
	Springs in the Hauran Plateau, Syria	Mainly basalts; limestones	Kattan (1996)
	Wells in the Hauran Plateau, Syria	Cretaceous limestones	Kattan (1996)
5d	Sedimentary rocks containing carbonates		
	North German Basin	Pleistocene sediments	Tesmer et al. (2007), Möller et al. (2007)
	Bohemian Massif	Metagabbros and amphibolites	Paces (1972), Paces (1987)
	Springs of the Altiplano, Chile	Sediments and acid volcanism	Morteani et al. (2014)
	Mississippi Salt Dome Basin, USA	Granite, granodiorites, amphibolites, phyllites, sst	Kharaka et al. (1987)

Table 4: *Information on groundwaters and brines plotted in Fig. 5.*

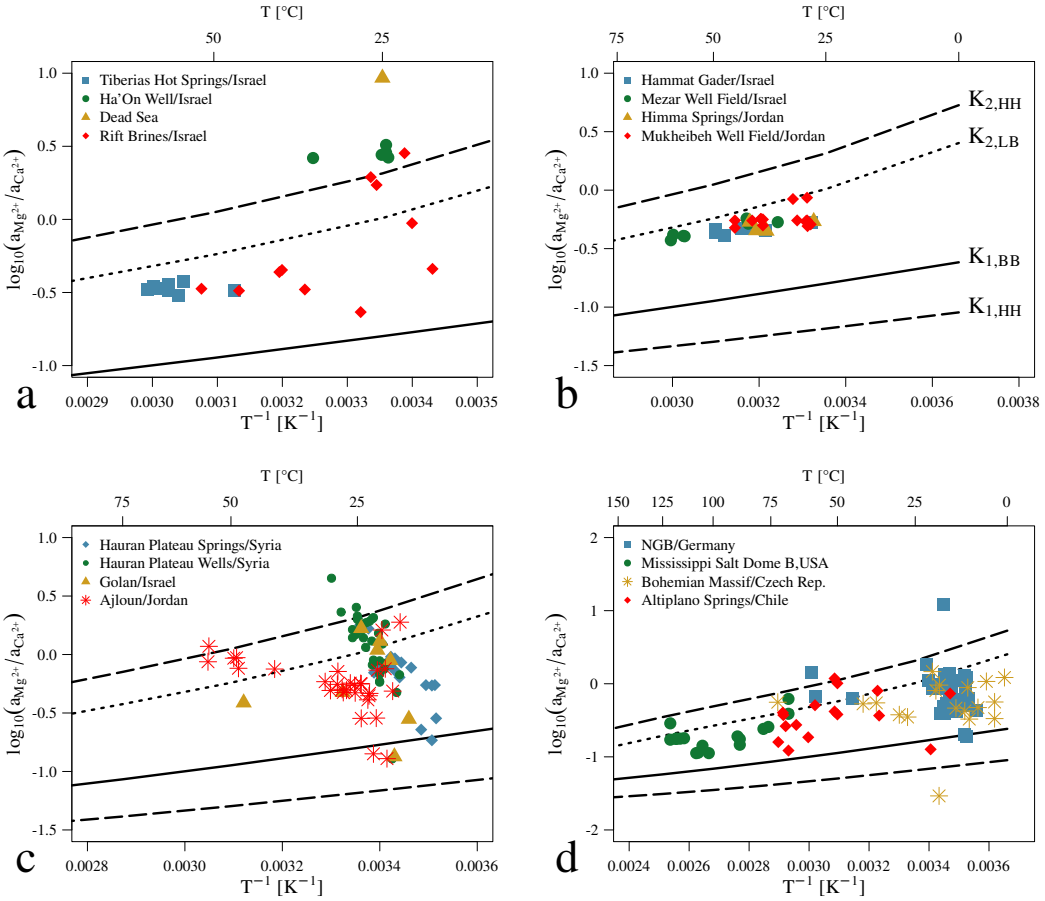

Fig. 5: $\mathrm{Log}_{10}({}^{a}\mathrm{Mg}^{2+}/{}^{a}\mathrm{Ca}^{2+})_{\mathrm{soln}}$ *as function of inverse absolute temperature. Average lithologies and sources of analyses are compiled in Table 2. (a) Brines from the Jordan Dead Sea Rift and the Red Sea Graben. Comparison of* $\log_{10}({}^{a}\mathrm{Mg}^{2+}/{}^{a}\mathrm{Ca}^{2+})_{\mathrm{soln}}$ *of Isreali brines from Ha'On well and Tiberias Hot Springs both being related to evaporation of seawater. For more details refer to subsection 3.2. Note that brines with* $\log_{10}({}^{a}\mathrm{Mg}^{2+}/{}^{a}\mathrm{Ca}^{2+})_{\mathrm{soln}}>0$ *do not form dolomite at the low temperatures of Ha'On and locally in the Rift. Although the environmental conditions in the Rift and the Graben are different,* $\log_{10}({}^{a}\mathrm{Mg}^{2+}/{}^{a}\mathrm{Ca}^{2+})_{\mathrm{soln}}$ *show a similar trend. (b) Groundwater and brines along the Yarmouk Gorge, Israel and Jordan. (c) Groundwater from limestones and basalts overlying the former in the Yarmouk Basin (Isreal, Jordan and Syria). The majority of data plot along a line similar to that in (b). (d) Groundwater and brines from carbonate bearing sediments and sedimentary rocks. Although many reactions other than in limestones are possible, the vertical spread of data is similar to that of (c).* $\mathrm{K}_{1,\mathrm{HH}}$ *and* $\mathrm{K}_{2,\mathrm{HH}}$ *are based on data from Helgeson et al. (1978);* $\mathrm{K}_{1,\mathrm{BB}}$ *results from data of Berman (1988);* $\mathrm{K}_{2,\mathrm{LB}}$ *is estimated from dissolution of disordered dolomite taken from "llnl.data" included in PHREEQC (Appelo et al., 2014) and dissolution of calcite after Berman (1988).*

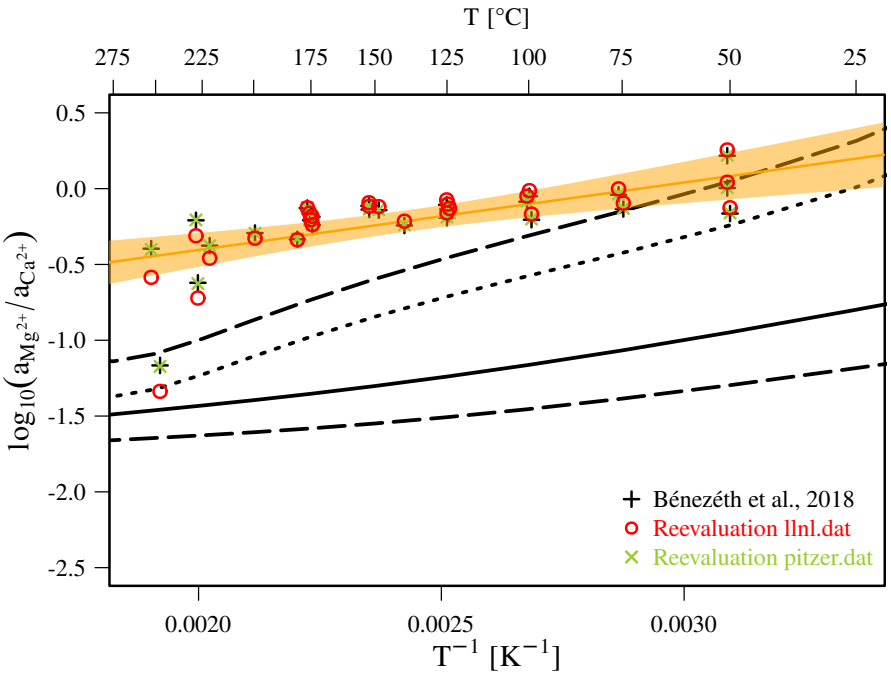

Fig. 6: *Comparison of* $\log_{10}({}^{a}Mg^{2+}/{}^{a}Ca^{2+})_{soln}$ *reported by Bénézeth et al. (2018), their reevaluation by PHREEQC using llnl.dat and pitzer.dat (Appelo et al., 2014) and thermodynamic estimates which are the same as given in Fig. 5.*

with dolomitic surface composition ($2 \cdot 8.2$; Fig. 3) but both show the same $\log_{10}({}^{a}Mg^{2+}/{}^{a}Ca^{2+})_{soln}$ values (Fig. 7).

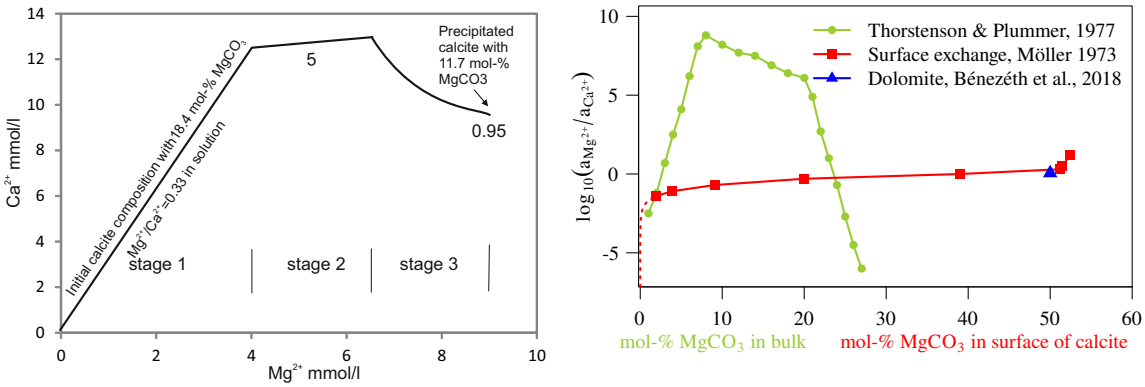

Fig. 7: *Dissolution of algae carbonates (HMC). (a) The composite trend is redrawn after Plummer and Mackenzie (1974). Figures below the trend are* Mg^{2+}/Ca^{2+} *values in solution; Beyond the trend initial and final compositions of high magnesium calcite are noted. (b) Comparison of* $\log_{10}({}^{a}Mg^{2+}/{}^{a}Ca^{2+})_{soln}$ *as function of mol-%* $MgCO_3$ *of bulk magnesian calcite (Thorstenson and Plummer, 1977) and of calcite surfaces after* Ca^{2+} *exchange against* Mg^{2+} *(Möller and Rajagopalan, 1972).* $\text{Log}_{10}({}^{a}Mg^{2+}/{}^{a}Ca^{2+})_{soln}$ *of dolomite at 25 °C is extrapolated from data reported by Bénézeth et al. (2018).*

3.4. Dissolution of high-magnesian calcite

Plummer and Mackenzie (1974) purported the dissolution kinetics of high magnesium calcite (HMC) of algae. The dissolution of HMC with a mean bulk composition of 18.4 mol-% $MgCO_3$ proceeds through

three stages (Fig. 7a). They are related to three different reactions with different rates: (stage 1) congruent dissolution, (stage 2) calcite growth on grain surfaces, whereas Ca^{2+} and Mg^{2+} are still released, and (stage 3) formation of incongruent Mg-calcite precipitate from solution. The reported final $^{a}Mg^{2+}/^{a}Ca^{2+}$ value in solution of steps 1, 2 and 3 increases from 0.3, 0.5 and finally to 0.95, respectively. Part of HMC with initial 18.4 mol-% $MgCO_3$ changes into final precipitate with 11.7 mol-% $MgCO_3$. In stage 3 equilibrium is not reached even after 670 hours. The final solution, however, requests a surface composition of about 30 mol-% $MgCO_3$ (Fig. 2a) of the algae HMC and the precipitated LMC, assuming that the surface of the algae HMC behaves similarly to pure LMC. In this case the surfaces of both minerals are higher in mol-% $MgCO_3$ than the average composition of the initial HMC of the algae. Thus, Mg^{2+} is still released from the bulk HMC during crystallization of LMC, although the surface seems to be higher in $MgCO_3$ than the bulk of the algae HMC. Considering surface ion exchange we would explain the whole process differently:

Stage 1: rapid incongruent dissolution, followed by

Stage 2: slowed-down incongruent dissolution of HMC associated with still increasing mol-% $MgCO_3$ of the surface and slightly increasing $(Mg^{2+}/Ca^{2+})_{soln}$, and

Stage 3: slow recrystallization during which bulk Mg^{2+} is still exchanging against Ca^{2+} from solution i.e., the amounts of Mg^{2+} increasing in solution equals the amount of Ca^{2+} decreasing in solution.

Thorstenson and Plummer (1977) derived $\log_{10}(^{a}Mg^{2+}/^{a}Ca^{2+})_{soln}$ based on the composition of HMC and thermodynamic data reported by Plummer and Mackenzie (1974) (Fig. 7b). Their $\log_{10}(^{a}Mg^{2+}/^{a}Ca^{2+})_{soln}$ data cover a range of 14 orders of magnitude. Calcite with dolomitic surface composition yields a similar $\log_{10}(^{a}Mg^{2+}/^{a}Ca^{2+})$ in solution like the dissolving dolomite (Fig. 7b).

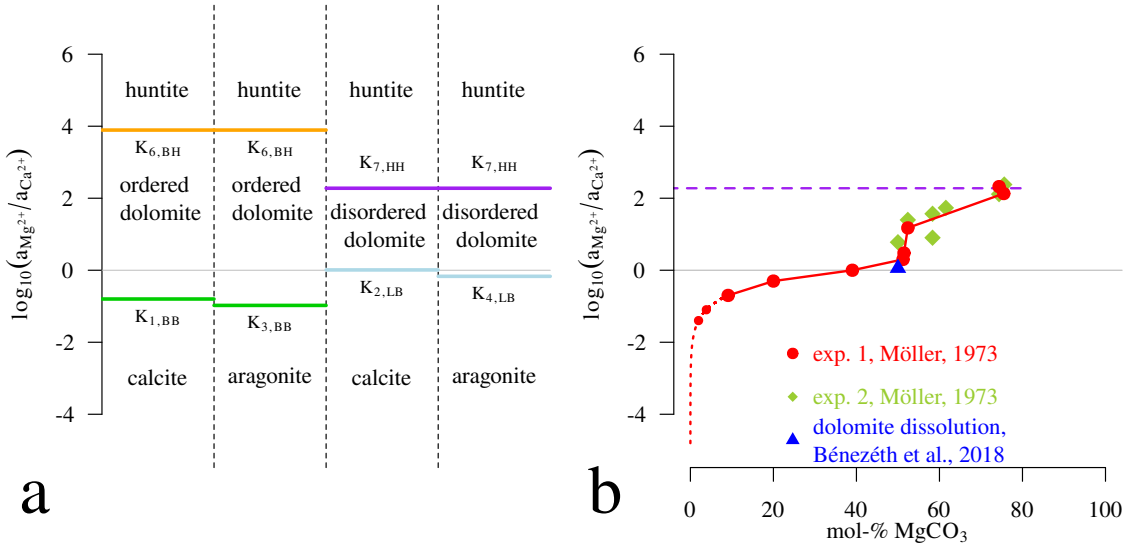

Fig. 8: *Comparison of* $\log_{10}(^{a}Mg^{2+}/^{a}Ca^{2+})_{soln}$ *of indicated carbonate mineral equilibria according the thermodynamical estimates (a) and of calcite undergoing surface exchange of* Ca^{2+} *against* Mg^{2+} *in solution (b). The* Mg^{2+} *content in the calcite surface is given in mol-%* $MgCO_3$.

In view of ion exchange results in calcite surfaces, it is suggested that similar processes should also occur in the reported dissolution experiment of HMC. In Fig. 7a the corresponding data of HMC alteration during equilibration with solution are compared with the surface composition derived from the described experiments. Note that the decrease of Mg^{2+} content in the altered HMC is associated with increasing Mg^{2+}/Ca^{2+} in solution. Increasing Mg^{2+}/Ca^{2+} in solution yields increasing Mg^{2+}/Ca^{2+} in

surface layers of the forming magnesian calcite with less mol-% $MgCO_3$ than in the bulk. This leads to the phenomenon that Mg^{2+}/Ca^{2+} in the surface increases, whereas locally the surface–near bulk ratio decreases during recrystallization, indicating that the bulk ratios of Mg^{2+} and Ca^{2+} do not attain equilibrium with the surface ratios. Only the surface layer is in equilibrium with the aqueous phase. From this finding it follows that it is impossible to derive the bulk composition of any Ca-Mg carbonate from the composition of its aqueous phase because the bulk of the mineral is rarely equilibrated with the ambient solution. It is always the surface that equilibrates with the aqueous phase and that may be quite different from the bulk composition. Even by recrystallization equilibrium between the bulk and surface cannot be attained. $({}^{a}Mg^{2+}/{}^{a}Ca^{2+})_{soln}$ give no hint about the minerals that are involved in the equilibrium.

4. Discussion

Perfect stoichiometry is neither given for calcite nor for dolomite and many other anhydrous carbonate minerals in nature. The apparent thermodynamic ranges of stability of calcite, aragonite, dolomite, and huntite at 25 °C are given by $\log_{10}({}^{a}Mg^{2+}/{}^{a}Ca^{2+})$ in Fig. 8a. In detail the relations are much more complex. From bottom to top the formation of magnesian calcite or aragonite depends on Mg^{2+} concentrations. Aragonite only precipitates from Ca^{2+}-HCO_3^- solution containing several g/l of $MgCl_2$ (Kitano et al., 1962). Due to the high Mg^{2+} concentration in the Dead Sea, influshed calcite is converted into aragonite (Barkan et al., 2001). The disordered dolomite and HMC only form during diagenesis or by biogenic processes at significant lower temperatures than ordered dolomite. Disordered dolomite displays a smaller range than dolomite in Fig. 8a. Other aspects are that only magnesian calcite with less than 4 mol-% $MgCO_3$ (LMC) precipitates inorganically and the biogenic HMC is thermodynamically metastable but long lived. Next to dolomite, huntite is expected to form but nesquihonite precipitates at both low temperatures and water activity (Davies and Bubela, 1973; Zachmann, 1989). The final step would be magnesite, which however is a hydrothermal product (Zachmann, 1989).

Contrasting the above sequence, magnesian calcite covers the whole range of calcite to huntite by its adjustable surface composition (Fig. 8b). Its $\log_{10}({}^{a}Mg^{2+}/{}^{a}Ca^{2+})_{soln}$ as a function of mol-% of $MgCO_3$ in the surface of calcite starts at very low values and increases to values of 2.3 in solution, i.e., huntitic surface composition of 0.75 mol-% $MgCO_3$. The corresponding $\log_{10}({}^{a}Mg^{2+}/{}^{a}Ca^{2+})_{soln}$ ratio is seemingly in agreement with the thermodynamic equilibrium of huntite (probably with disordered surface composition) and disordered dolomite and calcite at 25°C (Fig. 8b). This corresponds to the behaviour of dolomite dissolution, if disordered dolomite and not ordered dolomite is considered at equilibrium with LMC.

Calcite and LMC are common precipitates in solutions derived from weathering of any Ca^{2+}-bearing rock or sediment. Although the compiled groundwater and brines are from different areas (Table 4), they reveal that they all plot in a similar array of temperature and Mg^{2+}/Ca^{2+} (Fig. 5). Natural groundwater and brines cover the range of ${}^{a}Mg^{2+}/{}^{a}Ca^{2+}$ of -1.5 to +1.0, which includes the dependence on temperature, pH and the mineralogical composition of their catchment and aquifer rocks. The trend of Mg^{2+}/Ca^{2+} with temperature seems to follow that derived from thermodynamics (Figs. 5b and d). The solution should be in equilibrium with the surface composition of any mineral in the system; however, we are focussing on carbonates only. Thus, not the bulk of carbonates but only their surfaces determine the Mg^{2+}/Ca^{2+} in solution. If other reactions vary Mg^{2+} in solution, the surface composition will change accordingly. If for example in a basaltic catchment the Mg^{2+}/Ca^{2+} value is high due to weathering of olivine, where this water infiltrates underlying limestones, surface ion exchange is started and Mg^{2+}/Ca^{2+} is lowered. This exchange process goes on until the limestone surface has attained the same Mg^{2+}/Ca^{2+} value of the initial water. The amount of exchange at calcite surfaces determines the Mg^{2+}/Ca^{2+} values of the final groundwater. This means that aqueous Mg^{2+}/Ca^{2+} values cannot discriminate the origin of these waters.

In nature, however, dolostones and limestones are often part of the same aquifer. Groundwater passing both lithologies will finally show the latest equilibration with carbonate surfaces. Having in mind that surface compositions of magnesian calcite covers the whole range of $\log_{10}({}^{a}Mg^{2+}/{}^{a}Ca^{2+})$ of carbonates in sediments and weathered rocks, one can hardly expect to get precise information on distinct mineral equilibria from the composition of produced low-temperature fluids.

In studies of aqueous-solution/solid-solution relations in the low temperature system $CaO-MgO-CO_2-H_2O$, the surface composition of the solids is not considered. All thermodynamical

considerations assume that the bulk of carbonates equilibrates with the composition of the aqueous phase. Involvement of the bulk of minerals in equilibria would request a high mobility of ions in the carbonate lattices. The interdiffusion is however completely inhibited in solid solutions at ordinary temperatures (Lippmann, 1991). This is in agreement with self-diffusion experiments of ^{45}Ca in calcite which revealed that even over millions of years the composition of carbonates would not change to any appreciable extent (Brätter et al., 1972), and with field observations that arrangements of various HMC phases and dolomite survive geological periods (Land, 1985).

Unfortunately there is no detailed study on the temperature dependence of surface compositions of calcite or dolomite. However, data from Bénézeth et al. (2018) on dolomite dissolution reveal that even at 253°C no match with thermodynamically defined equilibria between both minerals is found. Only at 25°C the thermodynamical equilibria between disordered dolomite and calcite is seemingly established by their adjusted composition of surface layers of ordered dolomite and calcite.

The ion exchange in carbonate surfaces is associated with structural changes in the surface. These compositionally and structurally varied and charged surfaces are the base of the double layer established in solution. For instance, the Stern layer is the response to the interaction of components of the surface layer with opposite charged components in solution forming inner sphere complexes (Cappellen et al., 1993). The formation constants of these surface complexes are different for Ca^{2+}, Mg^{2+} and CO_3^{2-} in the surface and their corresponding counterparts in solution. The reported logK values are higher for Ca^{2+} surface complexes than for the corresponding Mg^{2+} species (Pokrovsky, 2001; Wolthers et al., 2008). The evaluation of logK values of the various reactions forming surface complexes, however did not consider variations in surface composition of minerals. Generalized, the surface composition and structure of incongruently dissolving carbonates such as dolomite, LMC, HMC or congruently dissolving carbonates such as calcite in solutions containing other divalent or trivalent ions are covered with a double layer the composition of which depends on that of the surface and on the ambient conditions such pH, CO_2 and additional components such as Na^+.

The hydration of Mg^{2+} plays a special role. At mineral surface, each exchanged Mg^{2+} ion still binds 1 H_2O. Because of the ionic size, the ion-dipole bond of $Mg^{2+}-H_2O$ is higher than that of $Ca^{2+}-H_2O$. The activation energy for removing surface water exceeds any energy being supplied from the ambient system. This slows down the growth rate of calcite. This inhibition effect is also the reason why dolomite and magnesite do not form at ambient temperatures even when more than enough Mg^{2+} is present, such as in seawater with a molar ratio of $^aMg^{2+}/^aCa^{2+}$ of 5:1. This behavior of Mg^{2+} ions is the reason why the sedimentary cover of the earth consists of mainly limestones and less of dolomite rocks besides sand- and claystones. If the Mg^{2+} would behave like Ca^{2+}, the world would look quite different: among the carbonates dolomite would be most frequent.

5. Conclusion

In this study the equilibration of differently composed carbonates is discussed in view of thermodynamical estimates and experimental results due to changes of surface composition of carbonates in solutions with Mg^{2+} at low temperatures. The equilibria between carbonates are described by $\log_{10}(^aMg^{2+}/^aCa^{2+})$ in solution. With few exceptions, it turns out that groundwater and brines irrespective to their sources plot between equilibria of either ordered dolomite–calcite or disordered dolomite-calcite. All these equilibria are controlled by exchange of Ca^{2+} against Mg^{2+} and possibly other auxiliary ions (Koss and Möller, 1974; Pokrovsky, 2001). Surface compositions of up to 75 mol-% $MgCO_3$ are easily achieved by calcite surfaces, thereby compositionally covering the range of carbonate minerals between calcite/aragonite and huntite. $Log_{10}(^aMg^{2+}/^aCa^{2+})$ of brines and groundwater from various siliceous and carbonaceous lithologies show a spread from -1.5 up to +1.0, identical with those of equilibria between stoichiometric carbonates.

In dissolution of HMC, Mg^{2+} content in the altered HMC decreases in association with increasing Mg^{2+}/Ca^{2+} in solution. Increasing Mg^{2+}/Ca^{2+} in solution leads to increasing Mg^{2+}/Ca^{2+} in surface layers of the forming magnesian calcite with less mol-% $MgCO_3$ than in the bulk. This leads to the phenomenon that Mg^{2+}/Ca^{2+} in the surface increases, whereas at other places the surface-near bulk ratio decreases due to recrystallization. Only the surface layer is in equilibrium with the aqueous phase indicating that it is impossible to derive the solubility of Ca-Mg carbonates from the composition of their aqueous phases because the bulk of the mineral is rarely equilibrated with the ambient solution. Even during recrystallization equilibrium between the bulk and varying surface composition cannot be

attained. In nature the bulk of carbonate minerals hardly if ever equilibrates with their ambient solutions due to extremely low diffusion of ions in the carbonate lattice.

The assumed incongruent dissolution of dolomite turned out as equilibrium of disordered dolomite and calcite, in other words, there is neither congruent dissolution of ordered dolomite nor equilibrium between ordered dolomite with calcite. In equilibrium, the solubility of the surface composition of disordered dolomite and magnesian calcite are the same.

Equilibrium between differently composed carbonates is attained when their surface compositions are in equilibrium with $^{a}Mg^{2+}/^{a}Ca^{2+}$ in solution. The bulk composition of carbonates cannot be derived from the Mg^{2+}/Ca^{2+} values of the common solution.

Acknowledgement

We highly acknowledge the comments of three anonymous reviewers which helped us improve the manuscript.

References

Andersson, M.P., Dideriksen, K., Sakuma, H., Stipp, S.L.S., 2016. Modelling how incorporation of divalent cations affects calcite wettability - implications for biomineralisation and oil recovery. Scientific Reports 6. doi:10.1038/srep28854.

Appelo, C., Parkhurst, D., Post, V., 2014. Equations for calculating hydrogeochemical reactions of minerals and gases such as CO_2 at high pressures and temperatures. Geochimica et Cosmochimica Acta 125, 49–67. doi:10.1016/j.gca.2013.10.003.

Arvidson, R., Mackenzie, F., 1999. The dolomite problem: Control of precipitation kinetics by temperature and saturation state. American Journal of Science 299, 257–288. doi:10.2475/ajs.299.4.257.

Baldermann, A., Deditius, A.P., Dietzel, M., Fichtner, V., Fischer, C., Hippler, D., Leis, A., Baldermann, C., Mavromatis, V., Stickler, C.P., Strauss, H., 2015. The role of bacterial sulfate reduction during dolomite precipitation: Implications from upper jurassic platform carbonates. Chemical Geology 412, 1–14. doi:10.1016/j.chemgeo.2015.07.020.

Barkan, E., Luz, B., Lazar, B., 2001. Dynamics of the carbon dioxide system in the dead sea. Geochimica et Cosmochimica Acta 65, 355–368. doi:10.1016/s0016-7037(00)00540-8.

Bénézeth, P., Berninger, U.N., Bovet, N., Schott, J., Oelkers, E.H., 2018. Experimental determination of the solubility product of dolomite at 50-253 °C. Geochimica et Cosmochimica Acta 224, 262–275. doi:10.1016/j.gca.2018.01.016.

Bergelson, G., Nativ, R., Bein, A., 1999. Salinization and dilution history of ground water discharging into the Sea of Galilee, the Dead Sea Transform, Israel. Applied Geochemistry 14, 91–118. doi:10.1016/s0883-2927(98)00039-0.

Berman, R.G., 1988. Internally-consistent thermodynamic data for minerals in the system Na_2O-K_2O-CaO-MgO-FeO-Fe_2O_3-Al_2O_3- SiO_2-TiO_2-H_2O-CO_2. Journal of Petrology 29, 445–522. doi:10.1093/petrology/29.2.445.

Berman, R.G., Brown, T.H., 1985. Heat capacity of minerals in the system Na_2O-K_2O-CaO-MgO-FeO-Fe_2O_3-Al_2O_3-SiO_2-TiO_2-H_2O-CO_2: representation, estimation, and high temperature extrapolation. Contributions to Mineralogy and Petrology 89, 168–183. doi:10.1007/bf00379451.

Berninger, U.N., Saldi, G.D., Jordan, G., Schott, J., Oelkers, E.H., 2017. Assessing dolomite surface reactivity at temperatures from 40 to 120 °C by hydrothermal atomic force microscopy. Geochimica et Cosmochimica Acta 199, 130–142. doi:10.1016/j.gca.2016.11.012.

Brätter, P., Möller, P., Rösick, U., 1972. On the equilibrium of coexisting sedimentary carbonates. Earth and Planetary Science Letters 14, 50–54. doi:10.1016/0012-821x(72)90078-7.

Cappellen, P.V., Charlet, L., Stumm, W., Wersin, P., 1993. A surface complexation model of the carbonate mineral-aqueous solution interface. Geochimica et Cosmochimica Acta 57, 3505–3518. doi:10.1016/0016-7037(93)90135-j.

Davies, P.J., Bubela, B., 1973. The transformation of nesquehonite into hydromagnesite. Chemical Geology 12, 289–300. doi:10.1016/0009-2541(73)90006-5.

Davis, K.J., 2000. The role of Mg^{2+} as an impurity in calcite growth. Science 290, 1134–1137. doi:10.1126/science.290.5494.1134.

Dick, J.M., 2019. CHNOSZ: Thermodynamic calculations and diagrams for geochemistry. Frontiers in Earth Science 7. doi:10.3389/feart.2019.00180.

Dobberschütz, S., Nielsen, M.R., Sand, K.K., Civioc, R., Bovet, N., Stipp, S.L.S., Andersson, M.P., 2018. The mechanisms of crystal growth inhibition by organic and inorganic inhibitors. Nature Communications 9. doi:10.1038/s41467-018-04022-0.

Generosi, J., Ceccato, M., Andersson, M.P., Hassenkam, T., Dobberschütz, S., Bovet, N., Stipp, S.L.S., 2016. Calcite wettability in the presence of dissolved Mg^{2+} and SO_4^{2-}. Energy And Fuels 31, 1005–1014. doi:10.1021/acs.energyfuels.6b02029.

Gledhill, D.K., Morse, J.W., 2006. Calcite solubility in Na-Ca-Mg-Cl brines. Chemical Geology 233, 249–256. doi:10.1016/j.chemgeo.2006.03.006.

Gregg, J.M., Bish, D.L., Kaczmarek, S.E., Machel, H.G., 2015. Mineralogy, nucleation and growth of dolomite in the laboratory and sedimentary environment: A review. Sedimentology 62, 1749–1769. doi:10.1111/sed.12202.

Gregg, J.M., Sibley, D.F., 1984. Epigenetic dolomitization and the origin of xenotopic dolomite texture. Journal of Sedimentary Research 54, 908–931. doi:10.1306/212f8535-2b24-11d7-8648000102c1865d.

Helgeson, H.C., Delany, J.M., Nesbitt, H.W., Bird, D.K., 1978. Summary and critique of the thermodynamic properties of rock-forming minerals. volume 278. American Journal of Science. URL: http://www.worldcat.org/oclc/13594862.

Helgeson, H.C., Kirkham, D.H., Flowers, G.C., 1981. Theoretical prediction of the thermodynamic behavior of aqueous electrolytes by high pressures and temperatures; IV, calculation of activity coefficients, osmotic coefficients, and apparent molal and standard and relative partial molal properties to 600 degrees C and 5kb. American Journal of Science 281, 1249–1516. doi:10.2475/ajs.281.10.1249.

Kattan, Z., 1996. Chemical and environmental isotope study of the fissured basaltic aquifer systems of Yarmouk Basin, Syria, in: Isotopes in Water Resources Management, Proceedings of a Symposium, Vienna 20-24 March 1995, pp. 3–27. IAEA-SM/336/28.

Kharaka, Y., Maest, A., Carothers, W., Law, L., Lamothe, P., Fries, T., 1987. Geochemistry of metal-rich brines from central Mississippi Salt Dome basin, U.S.A. Applied Geochemistry 2, 543–561. doi:10.1016/0883-2927(87)90008-4.

Kitano, Y., Park, K., Hood, D.W., 1962. Pure aragonite synthesis. Journal of Geophysical Research 67, 4873–4874. doi:10.1029/jz067i012p04873.

Koss, V., Möller, P., 1974. Oberflächenzusammensetzung, Löslichkeit und Ionenaktivitätsprodukt von Calcit in fremdionenhaltigen Lösungen. Zeitschrift für anorganische und allgemeine Chemie 410, 165–178. doi:10.1002/zaac.19744100210.

462 Krumgalz, B., 1997. Ion interaction approach to geochemical aspects of the Dead Sea, in: Tina, M.,
463 Ben-Avraham, Z., Gat, J. (Eds.), Dead Sea. The Lake and Its Settings.. Oxford University Press.
464 volume 36 of *Oxford Monographs on Geology and Geophysics.*, pp. 145–160.

465 Lakshtanov, L.Z., Belova, D.A., Okhrimenko, D.V., Stipp, S.L.S., 2014. Role of alginate in calcite
466 recrystallization. Crystal Growth & Design 15, 419–427. doi:10.1021/cg501492c.

467 Land, L.S., 1985. The origin of massive dolomite. Journal of Geological Education 33, 112–125. doi:10.
468 5408/0022-1368-33.2.112.

469 Land, L.S., 1998. Failure to precipitate dolomite at 25 °C from dilute solution despite 1000-fold
470 oversaturation after 32 years. Aquatic Geochemistry 4, 361–368. doi:10.1023/a:1009688315854.

471 Lippmann, F., 1991. Aqueous solubility of magnesian calcite with different endmembers. Acta
472 Mineralogica-Petrographica 32, 5–19.

473 Mavromatis, V., Gautier, Q., Bosc, O., Schott, J., 2013. Kinetics of Mg partition and Mg stable isotope
474 fractionation during its incorporation in calcite. Geochimica et Cosmochimica Acta 114, 188–203.
475 doi:10.1016/j.gca.2013.03.024.

476 Montanari, G., Rodriguez-Blanco, J.D., Bovet, N., Stipp, S.L.S., Tobler, D.J., 2017. Impact of citrate
477 ions on the nucleation and growth of anhydrous $CaCO_3$. Crystal Growth & Design 17, 5269–5275.
478 doi:10.1021/acs.cgd.7b00796.

479 Morteani, G., Möller, P., Dulski, P., Preinfalk, C., 2014. Major, trace element and stable isotope
480 composition of water and muds precipitated from the hot springs of bolivia: Are the waters of the
481 spring's potential ore forming fluids? Geochemistry 74, 49–62. doi:10.1016/j.chemer.2013.06.002.

482 Mucci, A., Morse, J.W., 1983. The incorporation of Mg^{2+} and Sr^{2+} into calcite overgrowths: influences
483 of growth rate and solution composition. Geochimica et Cosmochimica Acta 47, 217–233. doi:10.
484 1016/0016-7037(83)90135-7.

485 Möller, P., 1973. Determination of the composition of surface layers of calcite in solutions containing
486 Mg^{2+}. Journal of Inorganic and Nuclear Chemistry 35, 395–401. doi:10.1016/0022-1902(73)80550-0.

487 Möller, P., Rajagopalan, G., 1972. Cationic distribution and structural changes of mixed Mg-Ca layers on
488 calcite crystals. Zeitschrift für Physikalische Chemie 81, 47–56. doi:10.1524/zpch.1972.81.1-4.047.

489 Möller, P., Rajagopalan, G., 1976. Changes of excess free energies in the crystal growth processes of
490 calcite and aragonite due to the presence of Mg^{2+} ions in solution. Zeitschrift für Physikalische Chemie
491 99, 187–198. doi:10.1524/zpch.1976.99.4-6.187.

492 Möller, P., Rosenthal, E., Inbar, N., Siebert, C., 2009. Characterization of aquifer environments by major
493 and minor elements and stable isotopes of sulfate, in: Hoetzl, H., Möller, P., Rosenthal, E. (Eds.), The
494 Water of the Jordan Valley. Springer Verlag, Berlin, Heidelberg, pp. 75–121.

495 Möller, P., Rosenthal, E., Inbar, N., Siebert, C., 2018. Development of the Inland Sea and its
496 evaporites in the Jordan-Dead Sea Transform based on hydrogeochemical considerations and the
497 geological consequences. International Journal of Earth Sciences 107, 2409–2431. doi:10.1007/
498 s00531-018-1605-y.

499 Möller, P., Sastri, C.S., 1974. Estimation of the number of surface layers of calcite involved in Ca-^{45}Ca
500 isotopic exchange with solution. Zeitschrift für Physikalische Chemie 89, 80–87. doi:10.1524/zpch.
501 1974.89.1-4.080.

502 Möller, P., Siebert, C., Geyer, S., Inbar, N., Rosenthal, E., Flexer, A., Zilberbrand, M., 2011. Relationship
503 of brines in the Kinnarot Basin, Jordan-Dead Sea Rift Valley. Geofluids 12, 166–181. doi:10.1111/j.
504 1468-8123.2011.00353.x.

505 Möller, P., Weise, S.M., Tesmer, M., Dulski, P., Pekdeger, A., Bayer, U., Magri, F., 2007. Salinization of
506 groundwater in the North German Basin: results from conjoint investigation of major, trace element
507 and multi-isotope distribution. International Journal of Earth Sciences 97, 1057–1073. doi:10.1007/
508 s00531-007-0211-1.

Möller, P., Woith, H., Dulski, P., Lüders, V., Erzinger, J., Kämpf, H., Pekdeger, A., Hansen, B., Lodemann, M., Banks, D., 2005. Main and trace elements in KTB-VB fluid: composition and hints to its origin. Geofluids 5, 28–41. doi:10.1111/j.1468-8123.2004.00104.x.

Nielsen, M.R., Sand, K.K., Rodriguez-Blanco, J.D., Bovet, N., Generosi, J., Dalby, K.N., Stipp, S.L.S., 2016. Inhibition of calcite growth: Combined effects of Mg^{2+} and SO_4^{2-}. Crystal Growth & Design 16, 6199–6207. doi:10.1021/acs.cgd.6b00536.

Paces, T., 1972. Chemical characteristics and equilibration in natural water-felsic rock-CO_2 system. Geochimica et Cosmochimica Acta 36, 217–240. doi:10.1016/0016-7037(72)90007-5.

Paces, T., 1987. Hydrochemical evolution of saline waters from crystalline rocks of the Bohemian Massif (Czechoslovakia), in: Fritz, P., Frape, S. (Eds.), Saline water and gases in crystalline rocks. Geological Association of Canada Special Paper. volume 33, pp. 217–240.

Perez-Fernandez, A., Berninger, U.N., Mavromatis, V., von Strandmann, P.P., Oelkers, E., 2017. Ca and Mg isotope fractionation during the stoichiometric dissolution of dolomite at temperatures from 51 to 126 °C and 5 bars CO_2 pressure. Chemical Geology 467, 76–88. doi:10.1016/j.chemgeo.2017.07.026.

Pierret, M., Clauer, N., Bosch, D., Blanc, G., France-Lanord, C., 2001. Chemical and isotopic ($^{87}Sr/^{86}Sr$, δ18o, δD) constraints to the formation processes of red-sea brines. Geochimica et Cosmochimica Acta 65, 1259–1275. doi:10.1016/s0016-7037(00)00618-9.

Plummer, L., Busenberg, E., 1982. The solubilities of calcite, aragonite and vaterite in CO_2-H_2O solutions between 0 and 90°C, and an evaluation of the aqueous model for the system $CaCO_3$-CO_2-H_2O. Geochimica et Cosmochimica Acta 46, 1011–1040. doi:10.1016/0016-7037(82)90056-4.

Plummer, L., Mackenzie, F., 1974. Predicting mineral solubility from rate data; application to the dissolution of magnesian calcites. American Journal of Science 274, 61–83. doi:10.2475/ajs.274.1.61.

Pokrovsky, O.S., 2001. Kinetics and mechanisms of dolomite dissolution in neutral to alkaline solutions revisited. American Journal of Science 301, 597–626. doi:10.2475/ajs.301.7.597.

Pokrovsky, O.S., Golubev, S.V., Jordan, G., 2009a. Effect of organic and inorganic ligands on calcite and magnesite dissolution rates at 60 °C and 30 atm pCO_2. Chemical Geology 265, 33–43. doi:10.1016/j.chemgeo.2008.11.011.

Pokrovsky, O.S., Golubev, S.V., Schott, J., 2005. Dissolution kinetics of calcite, dolomite and magnesite at 25 °C and 0 to 50 atm pCO_2. Chemical Geology 217, 239–255. doi:10.1016/j.chemgeo.2004.12.012.

Pokrovsky, O.S., Golubev, S.V., Schott, J., Castillo, A., 2009b. Calcite, dolomite and magnesite dissolution kinetics in aqueous solutions at acid to circumneutral pH, 25 to 150 °C and 1 to 55 atm pCO_2: New constraints on CO_2 sequestration in sedimentary basins. Chemical Geology 265, 20–32. doi:10.1016/j.chemgeo.2009.01.013.

Raiteri, P., Demichelis, R., Gale, J.D., 2015. Thermodynamically consistent force field for molecular dynamics simulations of alkaline-earth carbonates and their aqueous speciation. The Journal of Physical Chemistry C 119, 24447—24458. URL: http://dx.doi.org/10.1021/acs.jpcc.5b07532, doi:10.1021/acs.jpcc.5b07532.

Sastri, C., Möller, P., 1974. Study of the influence of Mg^{2+} ions on Ca-^{45}Ca isotope exchange on the surface layers of calcite single crystals. Chemical Physics Letters 26, 116–120. doi:10.1016/0009-2614(74)89099-8.

Siebert, C., Möller, P., Geyer, S., Kraushaar, S., Dulski, P., Guttman, J., Subah, A., Rödiger, T., 2014. Thermal waters in the Lower Yarmouk Gorge and their relation to surrounding aquifers. Geochemistry 74, 425–441. doi:10.1016/j.chemer.2014.04.002.

Tesmer, M., Möller, P., Wieland, S., Jahnke, C., Voigt, H., Pekdeger, A., 2007. Deep reaching fluid flow in the North East German Basin: origin and processes of groundwater salinisation. Hydrogeology Journal 15, 1291–1306. doi:10.1007/s10040-007-0176-y.

Thorstenson, D., Plummer, L.N., 1977. Equilibrium criteria for two-component solids reacting with fixed composition in an aqueous phase example, the magnesian calcites. American Journal of Science 277, 1203–1223. doi:10.2475/ajs.277.9.1203.

Wang, X., Chou, I.M., Hu, W., Yuan, S., Liu, H., Wan, Y., Wang, X., 2016. Kinetic inhibition of dolomite precipitation: Insights from Raman spectroscopy of Mg^{2+}-SO_4^{2-} ion pairing in $MgSO_4/MgCl_2/NaCl$ solutions at temperatures of 25 to 200°C. Chemical Geology 435, 10–21. doi:10.1016/j.chemgeo.2016.04.020.

Warren, J., 2000. Dolomite: occurrence, evolution and economically important associations. Earth-Science Reviews 52, 1–81. doi:10.1016/s0012-8252(00)00022-2.

Wolthers, M., Charlet, L., Cappellen, P.V., 2008. The surface chemistry of divalent metal carbonate minerals; a critical assessment of surface charge and potential data using the charge distribution multi-site ion complexation model. American Journal of Science 308, 905–941. doi:10.2475/08.2008.02.

Zachmann, D., 1989. Mg-carbonate deposits in freshwater environment, in: Möller, P. (Ed.), Magnesite: geology, mineralogy, geochemistry, formations of Mg-carbonates.. Monograph Series on Ore deposits, Gebrüder Bornträger Berlin, Stuttgart. volume 28, pp. 61–94.

Appendix A. Relationship between activities and concentrations in Mg^{2+}/Ca^{2+}

All samples displayed in figure 5 are compiled in an electronic file which can be obtained from the authors on request.

The same samples are plotted together in figure A.1 separated by their ionic strength of either I<1 (circles) or I>1 (laying crosses). Figure A.1a reveals that ionic strength has little influence on $\log_{10}({}^{a}Mg^{2+}/{}^{a}Ca^{2+})$. figure A.1b shows that the majority of brines and groundwater plot in the same array. The distribution of $\log_{10}({}^{a}Mg^{2+}/{}^{a}Ca^{2+})_{soln}$ in groundwaters and brines and its temperature dependence suggests that they are dominantly framed by the thermodynamic equilibria of disordered dolomite-calcite and ordered dolomite-calcite.

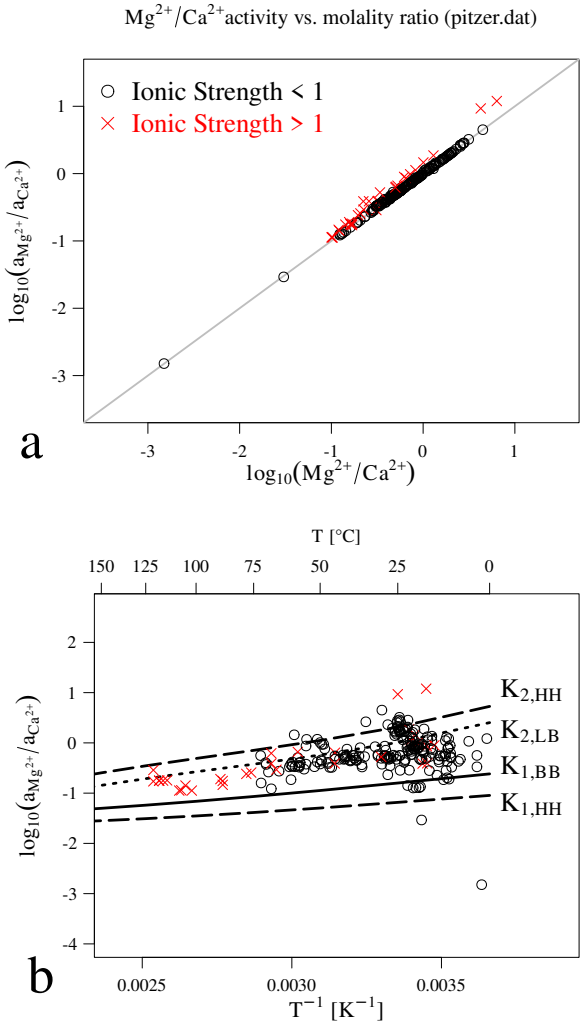

Fig. A.1: *Plot of all samples from figure 5 into an unique diagram but separating the samples according to their ionic strength. Circles and laying crosses represent ionic strength smaller or greater than unity, respectively.* ***(a)*** *Cross plots of activity and concentration ratios in groundwater and brines showing little difference between the two.* ***(b)*** *Cross plots of all samples in figure 5 showing no systematic differences with respect to ionic strength. The indices of reactions* K_i *are:* $K_{1,HH}$ *and* $K_{2,HH}$ *based on data from Helgeson et al. (1978);* $K_{1,BB}$ *results from data of Berman (1988);* $K_{1,LB}$ *is estimated from dissolution of disordered dolomite taken from PHREEQC's "llnl.dat" and dissolution of calcite after Berman (1988).*

Appendix B. Reevaluation of solubility experiments of Bénézeth et al., 2018

The experimental results of dolomite dissolution published by Bénézeth et al. (2018) have been reevaluated with the aid of PHREEQC models. The models have been constrained imposing the measured pH, total inorganic carbon, concentrations of Ca^{2+} and Mg^{2+} and by a background salinity of 0.0975 mol/kg Na^{+} and 0.1 mol/kg Cl^{-}. The aim was to determine activities of carbonate CO_3^{2-}, Ca^{2+} and Mg^{2+} following the extended Debye-Hückel and Pitzer activity theories, implemented respectively by the "llnl.dat" and "pitzer.dat" databases. The validity fields of these approaches are reported to be up to 300 °C and ionic strength around 2 mol/kg for NaCl dominated solutions in case of llnl.dat; and up to 200 °C and halite saturation for Pitzer. All data sets are fitted by the same linear model suggested by Bénézeth et al. (2018):

$$\log_{10}\left(\mathrm{IAP}\right)_{\mathrm{dol}} = a + b \cdot (1/T) + c \cdot T$$

with T in Kelvin. These fitted models are displayed as solid lines in figure B.1a. The speciation calculated by the diverse models result in lower $\log_{10}$(IAP) values of dolomite than -17.2 reported by the original authors, i.e., -17.8 and -17.5. More in detail, the discrepancy can be imputed to the calculated CO_3^{2-} concentrations, which are up to one order of magnitude lower than the reported measured values (figure B.1b) and to the calculated product of activity coefficients (figure B.1c).

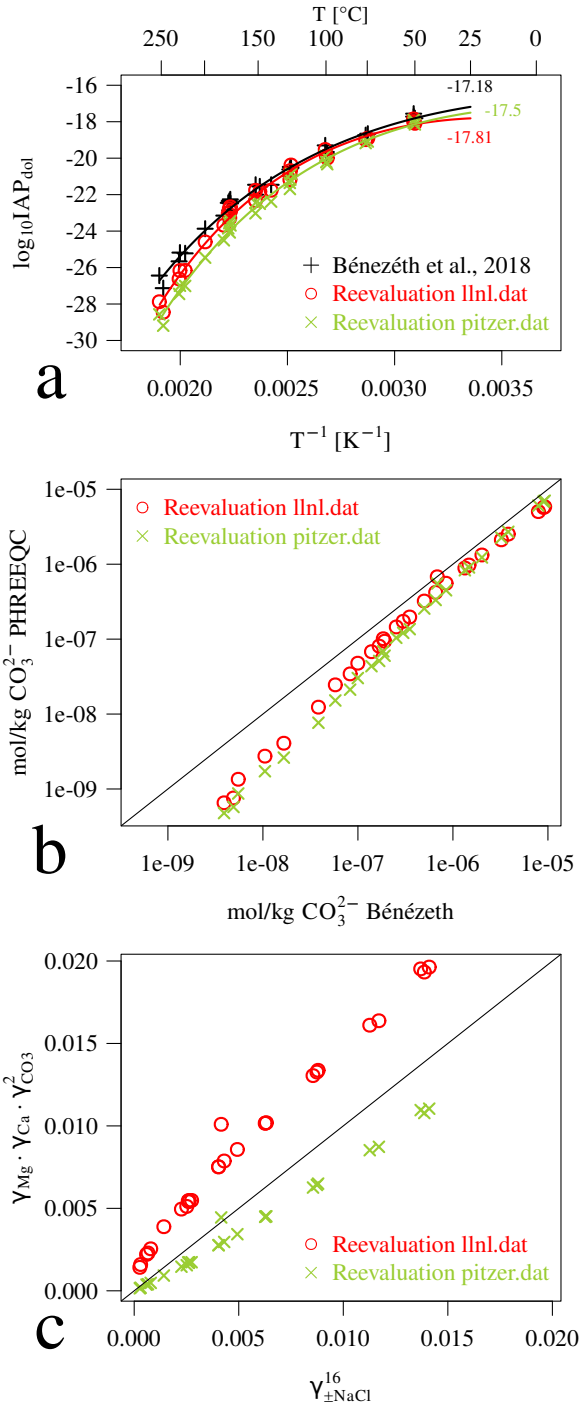

Fig. B.1: ***(a)*** *Reevaluation of* $\log_{10}(\mathrm{IAP})_{\mathrm{dol}}$ *by PHREEQC models using the databases llnl.dat and pitzer.dat from the data from Bénézeth et al. (2018);* ***(b)*** *comparison of* CO_3^{2-} *of and reevaluated* CO_3^{2-} *with PHREEQC;* ***(c)*** *the calculated products of activity coefficients according to llnl.dat and pitzer.dat are greater or lower than those used by Bénézeth et al. (2018).*